© 2021. Published by The Company of Biologists Ltd | Journal of Cell Science (2021) 134, jcs249276. doi:10.1242/jcs.249276

RESEARCH ARTICLE

SEC24A facilitates colocalization and Ca^{2+} flux between the endoplasmic reticulum and mitochondria

Tamutenda Chidawanyika[1], Rajarshi Chakrabarti[1], Kathryn S. Beauchemin[1], Henry N. Higgs[1] and Surachai Supattapone[1,2,*]

ABSTRACT

A genome-wide screen recently identified SEC24A as a novel mediator of thapsigargin-induced cell death in HAP1 cells. Here, we determined the cellular mechanism and specificity of SEC24A-mediated cytotoxicity. Measurement of Ca^{2+} levels using organelle-specific fluorescent indicator dyes showed that Ca^{2+} efflux from endoplasmic reticulum (ER) and influx into mitochondria were significantly impaired in *SEC24A*-knockout cells. Furthermore, *SEC24A*-knockout cells also showed ∼44% less colocalization of mitochondria and peripheral tubular ER. Knockout of *SEC24A*, but not its paralogs *SEC24B*, *SEC24C* or *SEC24D*, rescued HAP1 cells from cell death induced by three different inhibitors of sarcoplasmic/endoplasmic reticulum Ca^{2+} ATPases (SERCA) but not from cell death induced by a topoisomerase inhibitor. Thapsigargin-treated *SEC24A*-knockout cells showed a ∼2.5-fold increase in autophagic flux and ∼10-fold reduction in apoptosis compared to wild-type cells. Taken together, our findings indicate that SEC24A plays a previously unrecognized role in regulating association and Ca^{2+} flux between the ER and mitochondria, thereby impacting processes dependent on mitochondrial Ca^{2+} levels, including autophagy and apoptosis.

KEY WORDS: SEC24A, Calcium, SERCA, Thapsigargin, ER stress, Mitochondrial-associated membranes, Apoptosis, Autophagy

INTRODUCTION

Ca^{2+} is a key signaling molecule with multiple important cellular functions including the determination of cell fate (Berridge et al., 2000; Filippi-Chiela et al., 2016; Orrenius et al., 2003; Rizzuto and Pozzan, 2006). Therefore, Ca^{2+} levels in different organelles must be tightly regulated to maintain cellular homeostasis (Raffaello et al., 2016; Rizzuto and Pozzan, 2006).

The ER, which is an important intracellular Ca^{2+} store, must maintain micromolar levels of Ca^{2+} to ensure that Ca^{2+}-dependent chaperones can efficiently fold proteins in the ER (Bagur and Hajnóczky, 2017; Coe and Michalak, 2009). ER Ca^{2+} depletion activates the unfolded protein response (UPR) in an attempt to restore homeostasis, but if luminal ER Ca^{2+} levels are not replenished, cell death will ensue (Oslowski and Urano, 2011; Ron and Walter, 2007; Tabas and Ron, 2011; Xu et al., 2005). Similarly, mitochondrial Ca^{2+} levels must also be tightly regulated since mitochondria depend on Ca^{2+} to generate energy for cells, and Ca^{2+} levels in mitochondria determine whether they activate apoptosis or autophagy (Rizzuto et al., 1994; Rizzuto and Pozzan, 2006). Low mitochondrial Ca^{2+} levels result in low ATP levels, which in turn activate pathways to increase autophagy in an attempt to generate more energy for the cell (Cárdenas and Foskett, 2012; McCormack et al., 1990). Conversely, mitochondrial Ca^{2+} overload can be detrimental to the cell due to mitochondrial membrane permeabilization, which results in release of caspases and subsequent cell death (Carreras-Sureda et al., 2019; Orrenius et al., 2015; Qian et al., 1999).

Sarcoplasmic/endoplasmic reticulum Ca^{2+} ATPases (collectively SERCA) plays a critical role in the regulation of cellular Ca^{2+} homeostasis by actively pumping Ca^{2+} from the cytoplasm into the endoplasmic reticulum (ER) (Shigekawa et al., 1983; Spamer et al., 1987). SERCA inhibition can therefore have multiple downstream effects including ER stress induction, UPR activation, cellular Ca^{2+} perturbance, autophagy and cell death (Gordon et al., 1993). SERCA inhibitors such as thapsigargin, cyclopiazonic acid (CPA) and 2,5-di-tert-butylhydroquinone (DTBHQ) are often used to study the role of Ca^{2+} in cell biology (Goeger et al., 1988; Lytton et al., 1991; Moore et al., 1987; Oslowski and Urano, 2011). Given the effective cytotoxicity profile of SERCA inhibition, SERCA inhibitors can also be used as the active components of prodrugs used to treat some cancers (Mahalingam et al., 2016). Knowledge about exactly how SERCA inhibition can result in cell death as opposed to the other downstream effects will undoubtedly improve our understanding of SERCA and Ca^{2+} biology in cells, as well as provide new tools to study cell death pathways. Therapeutically, the identification of mediators that can prevent or potentiate cell death in cancers that can be treated by the prodrugs will also be useful.

Recently, we identified *SEC24A* as an essential mediator of thapsigargin-induced cell death in a CRISPR/Cas9 genome-wide screen in HAP1 cells (Chidawanyika et al., 2018), which are a haploid human leukemic cell line (Carette et al., 2011). We also found that SEC24A acts upstream of the UPR to mediate cell death from thapsigargin exposure (Chidawanyika et al., 2018). The canonical role of SEC24A in cells is to serve as an adaptor protein for a subset of secretory proteins during COPII-mediated vesicle transport from the ER to the Golgi (Gürkan et al., 2006; Pagano et al., 1999; Tang et al., 1999; Wendeler et al., 2007). However, the novel mechanism through which SEC24A mediates cell death induced by SERCA inhibition remained unknown. Therefore, we sought to investigate the cellular mechanism and specificity of SEC24A-mediated cytotoxicity.

RESULTS

Only one SEC24 paralog is required for thapsigargin-induced cell death

Previous work in our lab showed that *SEC24A* is essential for thapsigargin-induced cell death (Chidawanyika et al., 2018).

[1]Department of Biochemistry and Cell Biology, Guarini School of Graduate and Advanced Studies, Hanover, NH 03755, USA. [2]Department of Medicine, Geisel School of Medicine at Dartmouth, Hanover, NH 03755, USA.

*Author for correspondence (supattapone@dartmouth.edu)

S.S., 0000-0001-9060-4550

Handling Editor: Jennifer Lippincott-Schwartz
Received 22 May 2020; Accepted 12 February 2021

Journal of Cell Science (2021) 134, jcs249276. doi:10.1242/jcs.249276

Since *SEC24A* is one of four different paralogs in the SEC24 family of proteins (Tang et al., 1999; Wendeler et al., 2007), we first wanted to determine whether the ability to mediate thapsigargin-induced cell death was specific to *SEC24A*, or alternatively whether any of the other paralogs, *SEC24B*, *SEC24C* and *SEC24D*, might also be able to serve a similar function. Therefore, we generated mutant cell lines of all four SEC24 paralogs using CRISPR-mediated gene editing. The *SEC24A* mutant is a confirmed knockout, *SEC24A* KO (Chidawanyika et al., 2018). Western blots for SEC24A–SEC24D confirmed that all four proteins were expressed in wild-type (WT) cells, but not in specific CRISPR-edited cell lines (Fig. S1). When we treated WT and mutant cells with thapsigargin, only *SEC24A* KO cells were able to confer resistance to thapsigargin-induced cell death as shown by the 60% survival in *SEC24A* KO cells compared to no survival seen in WT cells and in mutants of *SEC24B*, *SEC24C* and *SEC24D* (Fig. 1A). These data highlight the specificity of SEC24A in mediating thapsigargin-induced cell death.

SEC24A knockout specifically protects cells against cell death induced by SERCA inhibitors

We next sought to determine whether *SEC24A* knockout could protect HAP1 cells against cell death induced by inducers other than thapsigargin. We found that *SEC24A* KO cells were partially resistant to cell death induced by two other SERCA inhibitors, CPA and DTBHQ, showing survival rates of 10% and 6%, respectively (Fig. 1B,C). In contrast, WT cells and mutants of *SEC24B*, *SEC24C* and *SEC24D* showed no significant survival in response to these compounds (Fig. 1B,C).

On the other hand, when WT and mutant cells were exposed to a topoisomerase inhibitor, camptothecin (CPT), none of the cells, including *SEC24A* KO cells, appeared to survive (Fig. 1D). Taken

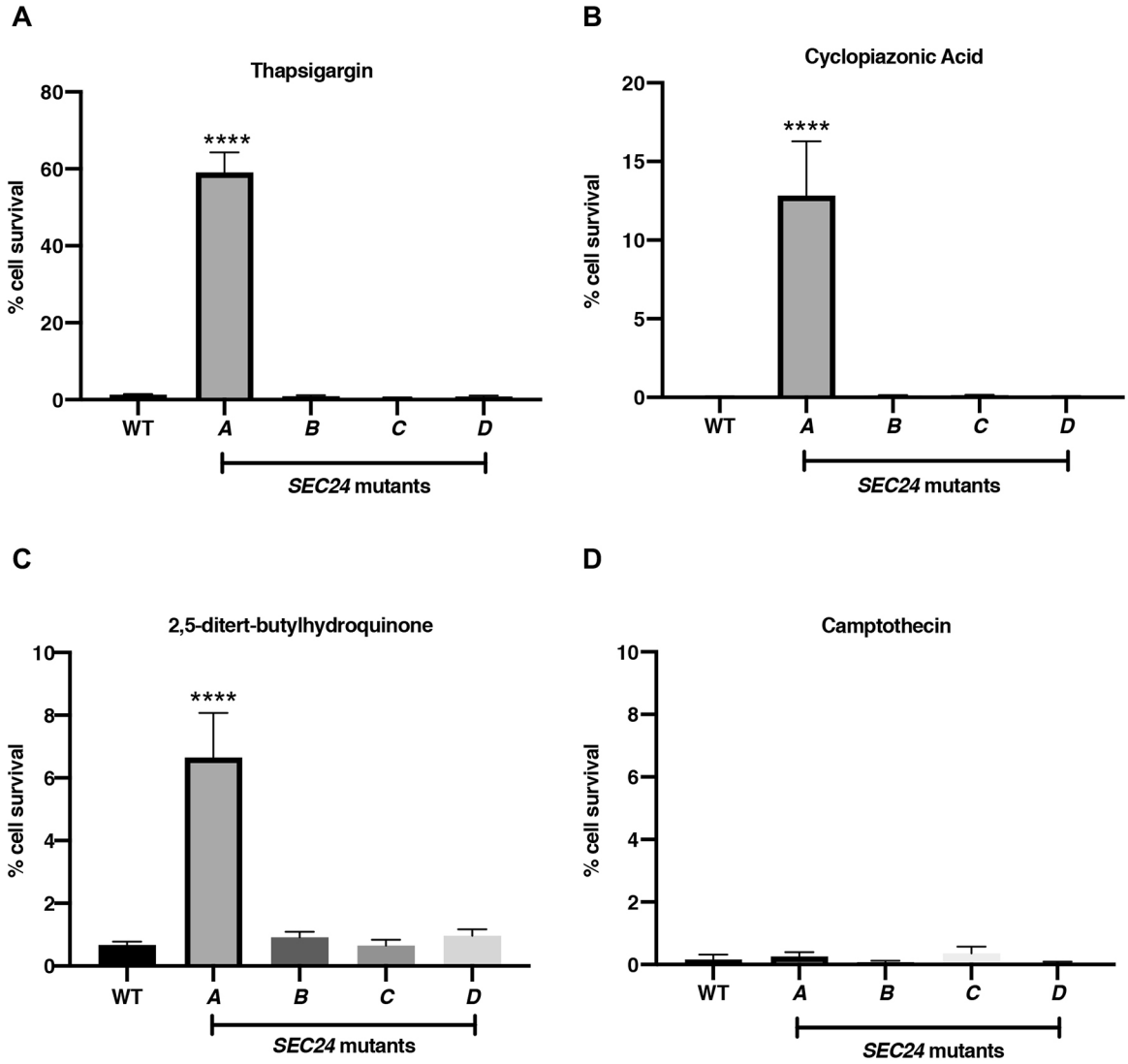

Fig. 1. Cytotoxic response of SEC24 paralog mutant cells to SERCA inhibitors and to DNA damage. WT and SEC24 paralog mutant HAP1 cells were treated with (A) 0.095 µM thapsigargin, (B) 80 µM cyclopiazonic acid, (C) 35 µM 2,5-di-tert-butylhydroquinone, or (D) 5 µM camptothecin, and assessed for cell survival using Trypan Blue after 3 days of treatment. Data are presented as mean±s.e.m. (*n*=6). ****P<0.0001 compared to WT cells (ordinary one-way ANOVA with Dunnett's multiple comparisons test).

Journal of Cell Science (2021) 134, jcs249276. doi:10.1242/jcs.249276

together, these results indicate that SEC24A specifically mediates cell death due to SERCA inhibition.

SEC24A knockout reduces Ca^{2+} depletion from ER and uptake by mitochondria

The ER is a crucial intracellular Ca^{2+} store that influences Ca^{2+} dynamics through its contacts with other organelles in the cell such as mitochondria, the plasma membrane and lysosomes (Burgoyne et al., 2015). The ER depends on SERCA to maintain a high ER luminal Ca^{2+} concentration by pumping Ca^{2+} from the cytoplasm into the ER lumen (Shigekawa et al., 1983; Spamer et al., 1987). Consequently, thapsigargin-induced SERCA inhibition can deplete ER Ca^{2+} stores and subsequently upset intracellular Ca^{2+} dynamics between the ER and different organelles (Raffaello et al., 2016; Rizzuto and Pozzan, 2006). To determine how *SEC24A* affects Ca^{2+} dynamics in different organelles in response to SERCA inhibition, we used the organelle-specific Ca^{2+} fluorescent probes, ER-GCamp6-150, mito-R-GECO1 and cyto-R-GECO1, to monitor changes in Ca^{2+} levels in the ER, mitochondria and cytoplasm, respectively, of WT and *SEC24A* KO cells treated with thapsigargin.

In both WT and *SEC24A* KO cells, the relative Ca^{2+} level in the ER decreased steadily over time following thapsigargin treatment, presumably because the ER lumen was unable to replenish Ca^{2+} due to SERCA inhibition (Fig. 2A,B). However, the rate of the decrease was significantly slower in the *SEC24A* KO cells compared to in the WT cells (Fig. 2B, red versus black line). Within 75 s of thapsigargin treatment, almost half of the Ca^{2+} in the WT cells had been depleted, while only about one-tenth of the Ca^{2+} from the ER in *SEC24A* KO cells had been depleted (from relative value of 1 to 0.9 in Fig. 2B). Additionally, the ER Ca^{2+} level eventually dropped to about one-third of the initial level (i.e. baseline level prior to thapsigargin treatment) in WT cells (Fig. 2B). In contrast, the ER Ca^{2+} level dropped to about half of the initial level in *SEC24A* KO cells, suggesting that the *SEC24A* KO cells are unable to empty the ER as efficiently as the WT cells (Fig. 2B). This inability of *SEC24A* KO cells to empty the ER as efficiently as WT cells was also seen when the cells were treated with another SERCA inhibitor, CPA, albeit with slower kinetics (Fig. S2A). In contrast, no difference was observed in ER emptying between the WT and *SEC24A* KO cells induced by a third SERCA inhibitor, DTBHQ (Fig. S2C). The reason for this discrepancy is unclear, but may be due to additional effects induced by DTBHQ that are not shared by the other inhibitors (Xu et al., 2004). Nonetheless, the differences in ER Ca^{2+} dynamics between thapsigargin- and CPA-treated WT and *SEC24A* KO cells suggest that SEC24A facilitates Ca^{2+} depletion from the ER.

When Ca^{2+} is emptied from the ER, it can enter different organelles, including the cytoplasm and mitochondria (at specialized sites where ER and mitochondria come into close proximity (Rizzuto et al., 2009; Rizzuto and Pozzan, 2006). In the cytoplasm of both the WT and *SEC24A* KO cells, sharp increases of cytoplasmic Ca^{2+} levels (three or more times the initial levels) were observed within 50 s of thapsigargin treatment, showing no significant differences between the two cell types (Fig. 2D). Similarly, cytoplasmic Ca^{2+} levels plateaued to ∼2-fold of the initial levels by 400 s after thapsigargin treatment in both cell types (Fig. 2C,D).

Thapsigargin treatment induced a delayed and gradual increase (∼1.3-fold) in mitochondrial Ca^{2+} levels in WT cells (Fig. 2F). Surprisingly, the mitochondria in *SEC24A* KO cells with respect to Ca^{2+} flux appeared to be completely unresponsive to thapsigargin treatment (Fig. 2F). When WT and *SEC24A* KO cells were treated with CPA or DTBHQ, the mitochondria displayed kinetic and phenotypic similarities to the mitochondria in thapsigargin-treated cells; WT mitochondria showed gradual Ca^{2+} uptake, while mitochondria of *SEC24A* KO seemed unresponsive to the different stimuli (Fig. S2B,D). These strikingly different responses in mitochondrial Ca^{2+} levels to thapsigargin, CPA, and DTBHQ treatments suggest that SEC24A might facilitate Ca^{2+} uptake into mitochondria.

SEC24A knockout reduces colocalization of mitochondria with tubular ER

Ca^{2+} signaling in the ER predominantly occurs in peripheral ER tubules (Schwarz and Blower, 2016; Shibata et al., 2010). Since *SEC24A* KO cells showed a defect in Ca^{2+} flux from the ER to mitochondria, we wondered whether the cause of this could be due to reduced contacts between ER tubules and mitochondria in *SEC24A* KO cells compared to WT cells. To investigate this, we used the organelle-specific fluorescent dyes ER-tagRFP and mito-BFP to visualize ER and mitochondria, respectively, and compared the degree of colocalization between tubular ER and mitochondria in WT, *SEC24A* KO and PTPIP51 OX cells, in which PTPIP51 (also known as RMDN3) is overexpressed as a positive control (Fig. 3A, B; Table 1). The proportion of colocalization in *SEC24A* KO cells was ∼44% less than in WT cells [5.31% in WT cells (Fig. 3B, top panel) versus 2.96% in *SEC24A* KO cells (Fig. 3B, middle panel, $^{****}P<0.0001$)] (Table 1). In PTPIP51 OX cells, where ER–mitochondria contacts are increased (Gomez-Suaga et al., 2017), we would expect to see an increase in colocalization proportions compared to WT cells if our method of evaluating ER–mitochondrial colocalizations is valid. Indeed, we found that colocalization proportions in PTPIP51 OX cells were ∼106% greater than in WT cells [5.31% in WT cells (Fig. 3B, top panel) versus 10.95% in PTPIP51 OX cells (Fig. 3B, bottom panel), $^{****}P<0.0001$] (Table 1). This finding validates our method of evaluating ER–mitochondrial colocalization.

To reduce the likelihood that our observations in the *SEC24A* KO cell line (generated using CRISPR editing) were due to off-target effects of the CRISPR editing, we examined colocalization proportions in two other *SEC24A* mutant cell lines, *SEC24A* mutant 1 and *SEC24A* mutant 4 (Chidawanyika et al., 2018). Compared to WT cells, both *SEC24A* mutant cell lines showed reduced colocalization proportions [5.31% in WT cells (Fig. 3B, top panel) versus 2.52% in *SEC24A* mutant 1 and 2.98% in *SEC24A* mutant 4 (Fig. S3B, top and bottom panels, respectively), $^{****}P<0.0001$] (Table 1). These results suggest that SEC24A plays an important role in maintaining contacts between tubular ER and mitochondria.

SEC24A knockout does not alter organelle morphology

Organelle Ca^{2+} flux can be affected by ER and mitochondrial morphology and vice versa (Jozsef et al., 2014; Kowaltowski et al., 2019). Since we observed a difference in ER Ca^{2+} uptake between WT and *SEC24A* KO cells, we used ER-tag RFP to assess ER morphology.

Peripheral ER is composed of sheets and tubules, which have distinct functions in cells (Schwarz and Blower, 2016). While tubules predominate in Ca^{2+} signaling, ER sheets are the major site of protein synthesis (Schwarz and Blower, 2016; Shibata et al., 2010). We wondered whether the observed differences in ER Ca^{2+} flux between WT and *SEC24A* KO cells might have been caused by changes in relative amounts of sheets and tubules in the cells. Visual examination of cells transfected with ER-tagRFP did not show any

Journal of Cell Science (2021) 134, jcs249276. doi:10.1242/jcs.249276

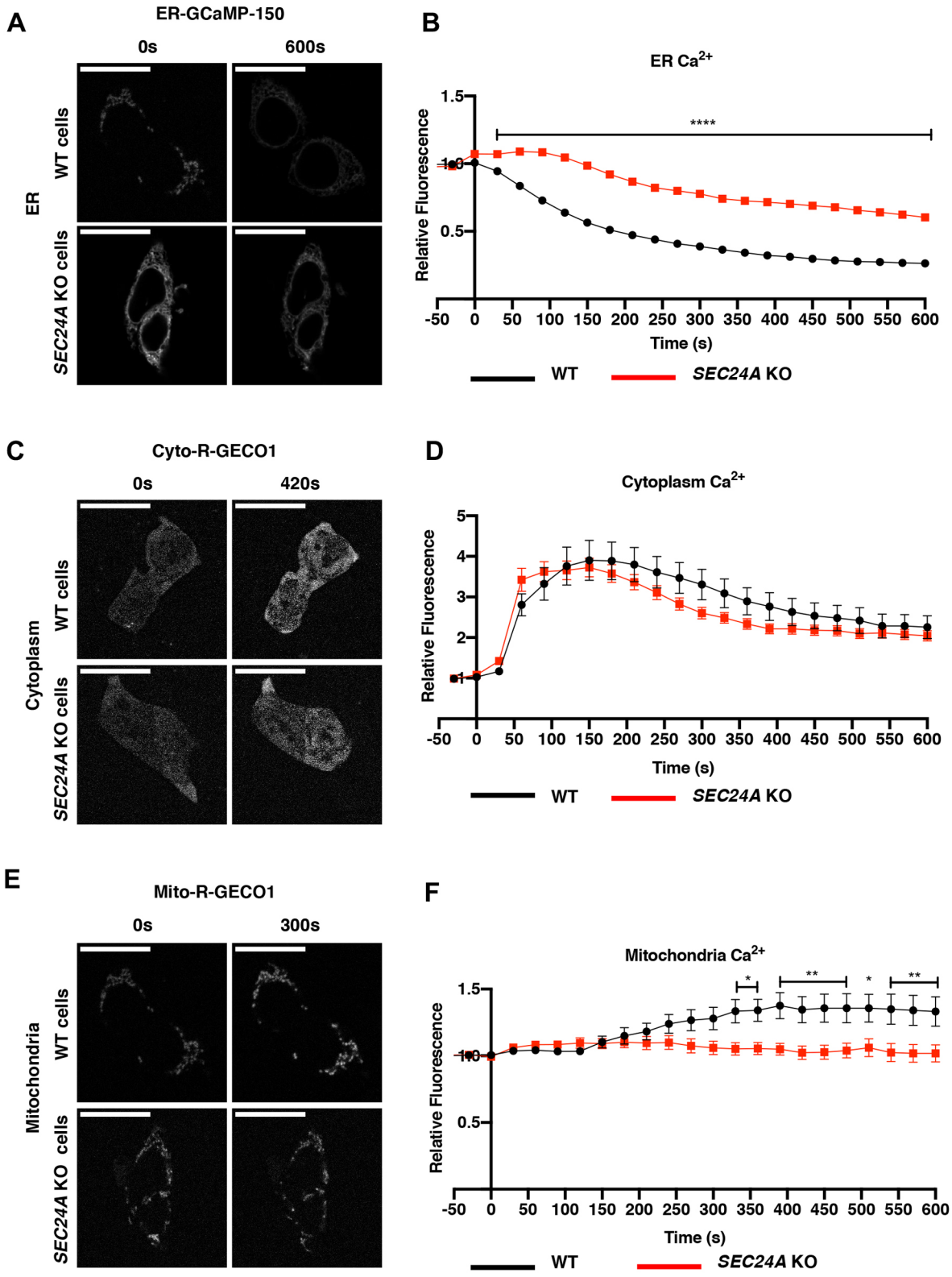

Fig. 2. Effects of SERCA inhibition on Ca^{2+} dynamics in different organelles of WT and *SEC24A* KO cells. The organelle-specific Ca^{2+} fluorescence-based probes, ER-GCamp6-150, Mito-R-GECO1 and Cyto-R-GECO, were used to measure Ca^{2+} levels in the ER, mitochondria, and cytoplasm, respectively, in WT and *SEC24A* KO cells with thapsigargin (TG) treatment. Representative images of WT and *SEC24A* KO cells showing Ca^{2+} levels in the (A) ER, (C) cytoplasm and (E) mitochondria at the indicated times after TG treatment. Scale bars: 20 µm. Quantitative representation of Ca^{2+} levels in the (B) ER (WT=47 cells, *SEC24A* KO=39 cells), (D) cytoplasm (WT=15 cells, *SEC24A* KO=54 cells), and (F) mitochondria (WT=20 cells, *SEC24A* KO=23 cells) cells. TG added at time=0 s. Relative fluorescence is a measure of Ca^{2+} levels and is calculated as F/F_0, where F_0 is baseline fluorescence and F is fluorescence at a specific time point in seconds, s, after TG treatment. Data are presented as mean±s.e.m. ****P<0.0001, **P<0.01, *P<0.05 compared to WT cells (two-way ANOVA tests with Šidák's multiple comparisons used to determine statistical differences between relative fluorescence values in WT and *SEC24A* KO cells at different time points).

Journal of Cell Science (2021) 134, jcs249276. doi:10.1242/jcs.249276

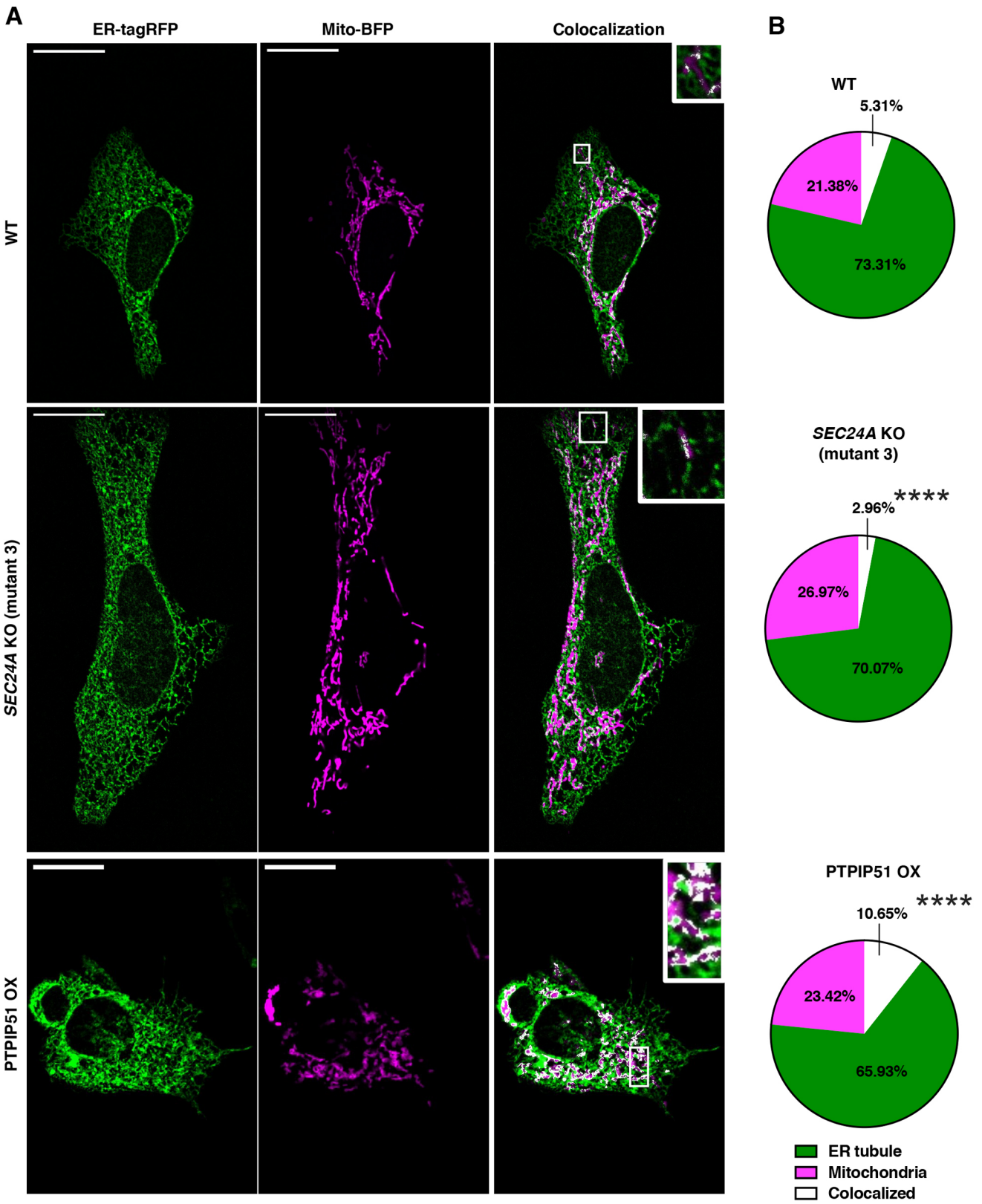

Fig. 3. Effects of *SEC24A* knockout on colocalization of ER tubules and mitochondria in WT, *SEC24A* KO, and PTPIP51 OX cells. WT, *SEC24A* KO (mutant 3) and PTPIP51 OX cells were transfected with ER-tagRFP and mito-BFP to visualize the ER and mitochondria, respectively. (A) Representative images showing false-colored ER (green) and mitochondria (magenta) in WT, *SEC24A* KO (mutant 3) and PTPIP51 OX cells. Areas of colocalization of ER and mitochondria are white. Insets show examples of areas (whites boxes) of peripheral ER tubules (100% zoom factor). Scale bars: 20 µm. (B) Quantifications of the proportions of peripheral ER tubules, mitochondria, and mitochondria colocalized with peripheral ER tubules in WT, *SEC24A* KO (mutant 3) and PTPIP51 OX cells. ****P<0.0001 [two-sided, two sample tests of proportions of colocalization were used to determine whether colocalization proportions in *SEC24A* KO (mutant 3) (12 cells) and PTPIP51 OX (10 cells) cells were significantly different compared to WT (12 cells)].

Journal of Cell Science (2021) 134, jcs249276. doi:10.1242/jcs.249276

Table 1. ER–mitochondria colocalization in different cell types

Cell type (*n*)	Colocalized pixels[a]	Total pixels[b]	Colocalized proportion[c]
WT (12)	4540	85,437	0.0531
SEC24A KO (12)	1601	54,167	0.0296****
PTPIP51 OX (10)	2764	25,959	0.106****
SEC24A mutant 1 (26)	362	14,364	0.0252****
SEC24A mutant 4 (27)	608	20,376	0.0298****

[a]Colocalized pixels are ER pixels that colocalized with mitochondrial pixels. [b]Total pixels=(total ER pixels excluding colocalized pixels)+(total mitochondrial pixels excluding colocalized pixels)+colocalized pixels. [c]Colocalized proportion=(colocalized pixels/total pixels). ****P<0.0001 (two-sided, two sample tests of proportions of colocalization to determine whether differences in proportions are statistically significant compared to WT cells).

apparent differences in the ER sheet-to-tubule ratios in the two cell types (red boxes for tubules, yellow boxes for sheets, Fig. 4A). These observations were confirmed by quantifications of western blots showing that the ratios of the levels of Climp63 [also known as CKAP4; exclusively found in ER sheets (Shibata et al., 2010)] to reticulon 4 (found in ER tubules; Jozsef et al., 2014) were not significantly different in WT cells compared to the levels in *SEC24A* KO cells, in the presence or absence of thapsigargin (TG) (Fig. 4B,C).

To examine mitochondrial morphology, we used mito-BFP to visualize the mitochondria in WT and *SEC24A* KO cells. We could not see any obvious differences in mitochondrial morphology in WT cells compared to *SEC24A* KO cells on visual examination (Fig. 5A). Next, we wondered whether differences in the length or number of mitochondria might be related to the differences that we observed in Ca^{2+} uptake in the mitochondria of the WT and *SEC24A* KO cells. There was no significant difference in mean area per mitochondrion, a measure of mitochondrial length (Lee et al., 2016), or in mean mitochondrial number in WT cells compared to *SEC24A* KO cells (Fig. 5B,C).

Together, these data show that *SEC24A* knockout does not cause gross alterations in ER or mitochondrial organellar morphology.

SEC24A knockout increases autophagic flux induced by thapsigargin treatment

We next sought to confirm our mitochondrial Ca^{2+} measurements by assaying a downstream process known to be dependent upon mitochondrial Ca^{2+} levels. It has been previously shown that low mitochondrial Ca^{2+} levels upregulate autophagy (Cárdenas and Foskett, 2012; McCormack et al., 1990), and therefore we hypothesized that autophagic flux should be higher in thapsigargin-treated *SEC24A* knockout cells (relative to WT cells) due to impaired mitochondrial Ca^{2+} uptake (Fig. 2F, red line). To test this hypothesis, we measured autophagic flux using a standard western blot assay based on the increase in the LC3B-II (lipidated LC3B, also known as MAP1LC3B) to LC3B-I (non-lipidated LC3B) ratio upon addition of bafilomycin A1 (Mizushima and Yoshimori, 2007; Mizushima et al., 2010).

There was no difference in autophagic flux in DMSO-treated WT and *SEC24A* KO cells since both cell types showed ∼2-fold increases in autophagic flux after bafilomycin A1 treatment (compare lanes 1 and 2 for WT cells and lanes 7 and 8 for *SEC24A* KO cells in Fig. S4A; DMSO-treated −BafA1 to +BafA1, black line for WT vs red line for *SEC24A* KO). Thapsigargin-treated *SEC24A* KO cells showed a ∼4-fold increase in autophagic flux (compare lanes 9 and 10 in Fig. S4A; TG-treated −BafA1 to +BafA1, red line in Fig. S4B) compared to a ∼1.5-fold increase in similarly treated WT cells (compare lanes 3 and 4 in Fig. S4A; TG-treated −BafA1 to +BafA1, black line in Fig. S4B). Thus, thapsigargin-treated *SEC24A* KO cells appear to have ∼2.5-fold greater rate of autophagic flux than WT cells.

The drug torin-1 (an inhibitor of mammalian target of rapamycin) is known to induce autophagy in cells (Gomez-Suaga et al., 2017). Previous studies have shown that torin-1-induced autophagic flux is reduced when ER–mitochondria contacts are increased (Gomez-Suaga et al., 2017). We hypothesized that the decreased mitochondrial Ca^{2+} uptake in *SEC24A* KO cells is due to decreased ER–mitochondria contacts as suggested by our colocalization experiments (Fig. 3B, middle panel, Table 1). If this is the case, we would expect torin-1 treatment to show greater autophagic flux in *SEC24A* KO cells compared to WT cells. Indeed, when cells were treated with torin-1, *SEC24A* KO cells showed a ∼8-fold increase in autophagic flux (compare lanes 11 and 12 in Fig. S4A; TRN1-treated −BafA1 to +BafA1, red line in Fig. S4B) compared to a ∼2-fold increase in WT cells (compare lanes 5 and 6 in Fig. S4A; TRN1-treated −BafA1 to +BafA1, black line in Fig. S4B). Thus, torin-1-treated *SEC24A* KO cells have a 4-fold greater rate of autophagic flux than WT cells, presumably due to decreased ER–mitochondria contacts in *SEC24A* KO cells.

Our findings are consistent with and support the observations that SEC24A plays an important role in maintaining contacts between tubular ER and mitochondria, and that thapsigargin-treated *SEC24A* KO cells have impaired mitochondrial Ca^{2+} uptake.

Thapsigargin-induced apoptosis is inhibited in *SEC24A* knockout cells

It is known that mitochondrial Ca^{2+} overload can open the mitochondrial permeability transition pore, leading to caspase activation and apoptosis (Qian et al., 1999). Since thapsigargin fails to induce mitochondrial Ca^{2+} uptake or cell death in *SEC24A* KO cells, we hypothesized that thapsigargin might trigger apoptosis in WT cells but not in *SEC24A* KO cells. To test this hypothesis, we first tested whether thapsigargin can induce apoptosis in HAP1 cells. When WT HAP1 cells were treated with 0.095 µM thapsigargin after a pre-treatment with DMSO, only ∼20% of the cells survived the treatment (Fig. 6A). Interestingly, without a DMSO pre-treatment, almost no WT cells survive treatment with 0.095 µM thapsigargin (Fig. 2A). The discrepancy in thapsigargin-induced cytotoxicity is likely due to the DMSO pre-treatment resulting in resistance to cytotoxicity since DMSO has been previously shown to affect cellular death pathways (Kita et al., 2015; Verheijen et al., 2019). When WT cells were treated with thapsigargin and a pan-caspase inhibitor (Q-VD-OPh), cell survival increased, with 60% of the cells surviving the treatment (Fig. 6A). Similar results were obtained with CPT (Fig. 6A), a known apoptosis inducer (Chen and Liu, 1994; Sanchez-Alcazar et al., 2000; Traganos et al., 1996). These data show that thapsigargin induces cell death in HAP1 cells through a caspase-dependent process, most likely apoptosis.

A hallmark of cells undergoing apoptosis is the caspase-dependent cleavage of PARP from a large precursor (116 kDa) into shorter fragments, one of which is 89 kDa (Kaufmann et al., 1993; Le Rhun et al., 1998). In order to determine whether *SEC24A* KO cells undergo apoptosis after thapsigargin treatment, we collected lysates from WT and *SEC24A* KO cells treated with either thapsigargin or CPT. When WT and *SEC24A* KO cells were treated with thapsigargin, PARP cleavage in WT cells was significantly greater than that in *SEC24A* KO cells, which had negligible amounts of PARP cleavage [Fig. 6B compare lanes 3 and 9 (red arrows), and Fig. 6C, compare cleavage values of 0.21 to ∼0].

Journal of Cell Science (2021) 134, jcs249276. doi:10.1242/jcs.249276

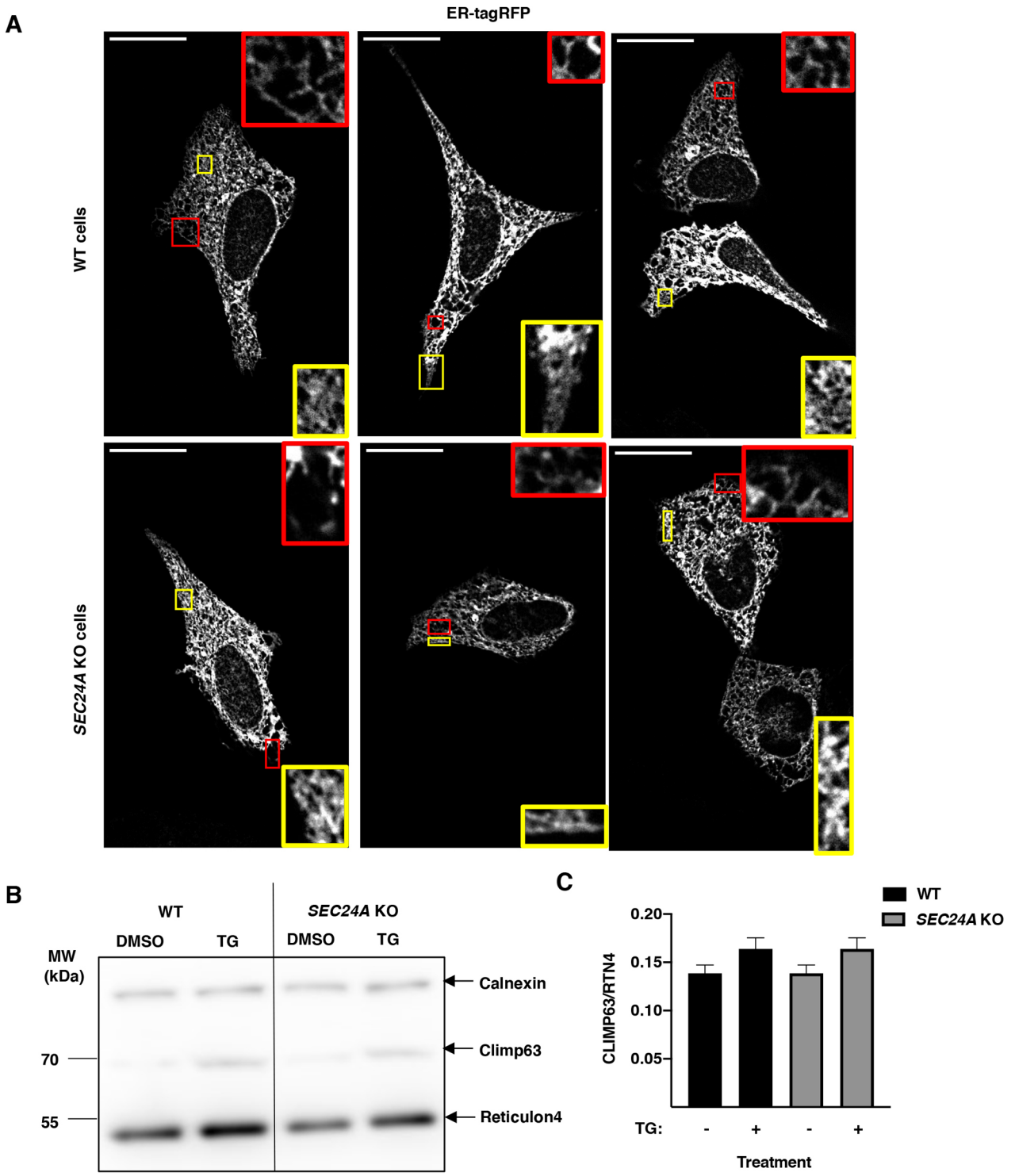

Fig. 4. Effect of *SEC24A* knockout on morphology of ER in cells. WT and *SEC24A* KO cells were transfected with ER-tagRFP to visualize the ER. Images of (A) ER morphology in representative WT and *SEC24A* KO cells. Insets highlighted with a red box show examples of peripheral ER tubules, while insets highlighted with a yellow box show examples of peripheral ER sheets (both at 150% zoom factor). Scale bars: 20 µm. (B) Western blot of Climp63 and reticulon4 (RTN4) proteins as representatives of sheet and tubular ER, respectively, with and without thapsigargin (TG) treatment. Calnexin is used as the loading control. (C) Quantification of the ER-sheet-to-tubule ratios in B represented by the ratios of Climp63 to RTN4 in WT and *SEC24A* KO cells in the presence or absence of thapsigargin (TG). Data are presented as mean±s.e.m. (n=5 experiments of three biological replicates and one or two technical replicates).

In contrast, CPT treatment in WT and *SEC24A* KO cells resulted in PARP cleavage levels that were not significantly different (Fig. 6B, compare lanes 5 and 11, and Fig. 6C, compare cleavage values of 0.3 to ∼0.2), suggesting that both cell types undergo apoptosis efficiently in response to CPT. These findings show that *SEC24A* is specifically required for apoptosis induced by thapsigargin, but not CPT, and are consistent with the differential susceptibility of *SEC24A* knockout cells to these two agents (Fig. 1D).

Journal of Cell Science (2021) 134, jcs249276. doi:10.1242/jcs.249276

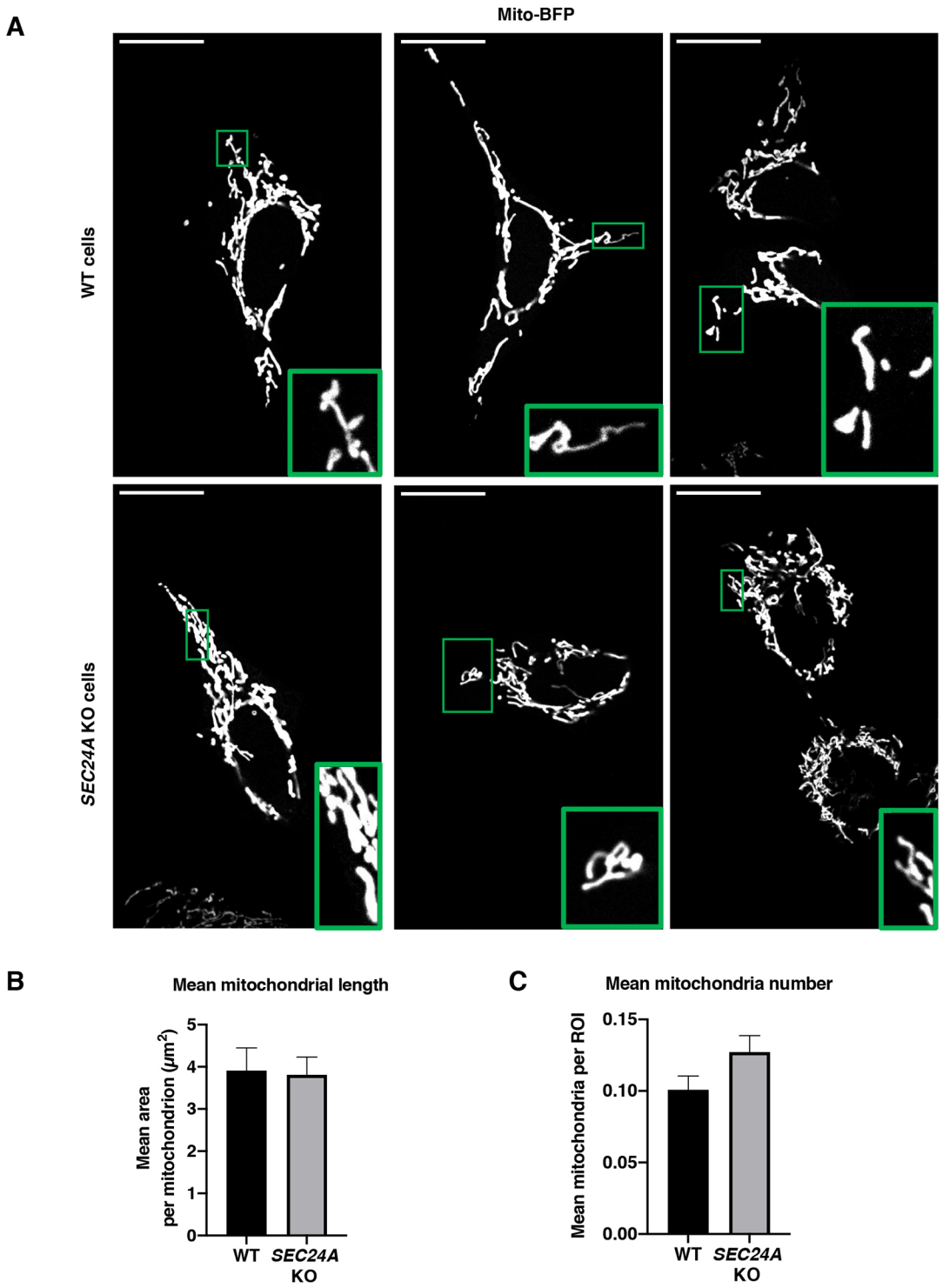

Fig. 5. Effect of *SEC24A* knockout on morphology of mitochondria in cells. WT and *SEC24A* KO cells were transfected with mito-BFP to visualize the mitochondria. Images of (A) mitochondria in representative WT and *SEC24A* KO cells. Insets (green boxes) show examples of mitochondria in the periphery of the cells (100% zoom factor). Scale bars: 20 µm. (B) Quantification of mean±s.e.m. mitochondrial length represented as mean area per mitochondrion in WT and *SEC24A* KO cells. (C) Quantification of mean±s.e.m. mitochondria number represented as mean mitochondria per ROI in WT and *SEC24A* KO cells. (*n*=23 WT cells, 35 *SEC24A* KO cells).

DISCUSSION

In this study, we initially sought to characterize how SEC24A mediates thapsigargin-induced cell death in HAP1 cells. Surprisingly, we discovered that SEC24A facilitates Ca^{2+} flux and contacts between the ER and the mitochondria of HAP1 cells. As a consequence of reduced mitochondrial Ca^{2+} influx, *SEC24A* KO cells treated with SERCA inhibitors display increased autophagy and decreased apoptosis, leading to cell survival.

Journal of Cell Science (2021) 134, jcs249276. doi:10.1242/jcs.249276

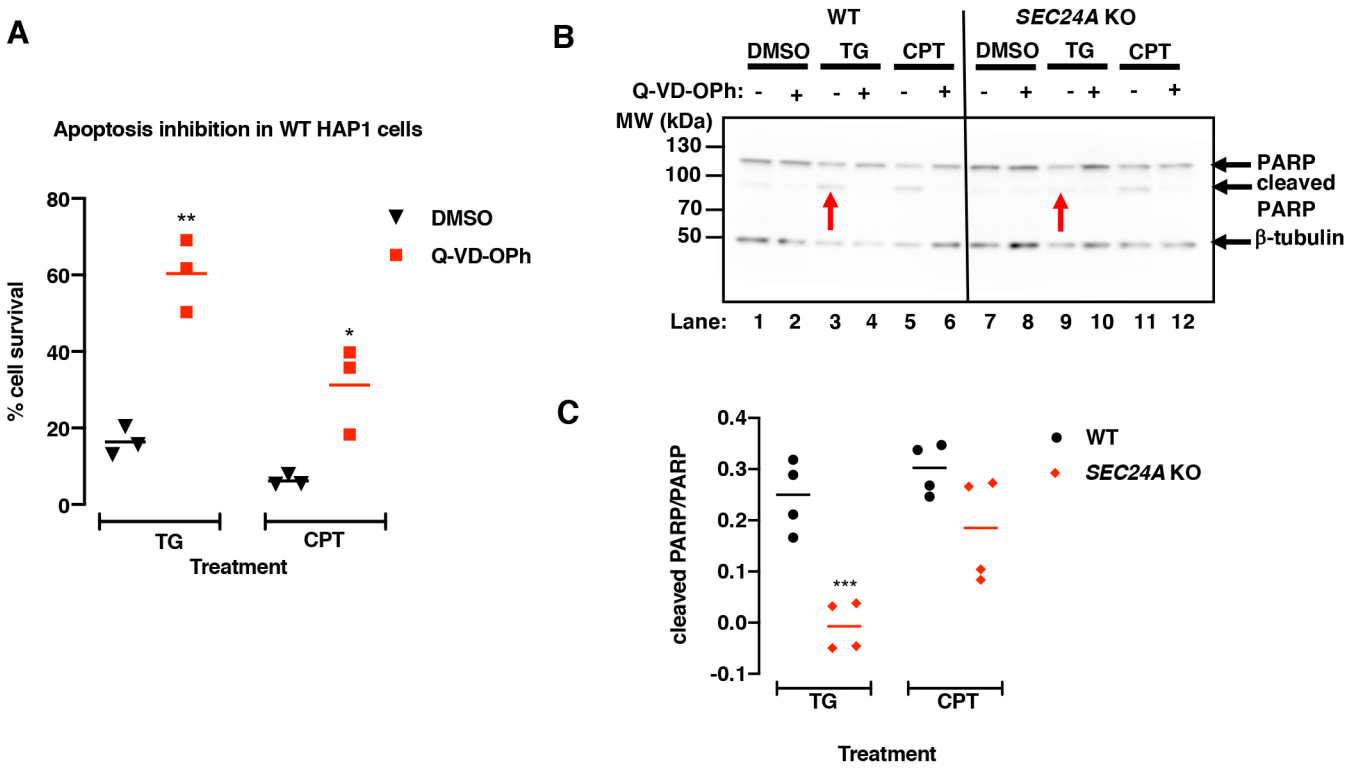

Fig. 6. Effect of SERCA inhibition on apoptosis in WT and *SEC24A* KO cells. (A) WT cells were pre-treated with 400 µM Q-VD-OPh or DMSO for 1 h before treatment with thapsigargin (TG), camptothecin (CPT) or DMSO to attain final concentrations of 0.095 µM thapsigargin (TG) or 5 µM camptothecin (CPT) in the presence of 200 µM Q-VD-OPh or DMSO. Assessment of cell survival after 3 days of treatment using Trypan Blue. Data are presented as mean±s.e.m. (*n*=3 independent experiments). ***P*<0.002, **P*<0.02 compared to DMSO-treated cells (unpaired two-tailed *t*-test). (B) Western blot of PARP cleavage in WT and *SEC24A* KO cells to monitor apoptosis after a 24 h treatment. β-tubulin is used as the loading control. Red arrows indicate cleaved PARP in samples treated with thapsigargin (TG). (C) Quantification of apoptosis in B represented by the ratio of cleaved PARP to uncleaved PARP in WT and *SEC24A* KO cells treated with TG or CPT. Data are presented as mean±s.e.m. (*n*=4 independent experiments). ****P*=0.001 compared to WT cells (unpaired two-tailed *t*-test).

SEC24A modulates Ca^{2+} flux from the ER and mitochondria through facilitating contacts between the organelles

Most interestingly, we discovered that SEC24A specifically facilitates Ca^{2+} flux from ER to mitochondria in response to thapsigargin treatment. Thapsigargin-induced ER Ca^{2+} depletion is caused by the inability of SERCA to actively transport Ca^{2+} from the cytoplasm into the ER, resulting in a net movement of Ca^{2+} from the ER into the cytoplasm and mitochondria through leak channels such as the inositol-1,4,5-triphosphate receptor (IP3R) and presenilins (Kiviluoto et al., 2013; Rizzuto and Pozzan, 2006; Supattapone et al., 1988). Our data suggest that SEC24A facilitates the function of a subset of these channels since less Ca^{2+} leaves the ER in *SEC24A* KO cells. Since cytoplasmic Ca^{2+} levels are similar in WT and *SEC24A* KO cells, Ca^{2+} flux from the ER into bulk cytoplasm appears to be unaffected by SEC24A. Rather, we infer that the affected leak channels control Ca^{2+} flux from the ER to the mitochondria, and that the SEC24A-mediated movement of Ca^{2+} into the mitochondria results in apoptosis (Pinton et al., 2008).

The transfer of Ca^{2+} between the ER and mitochondria occurs through mitochondrial-associated membranes (MAMs) which are micro-domains formed by proteins on both organelles (Rizzuto et al., 2009; Rizzuto and Pozzan, 2006). Of note, our data highlighted two important functions of SEC24A that suggest a role for SEC24A in formation and or function of MAMs. We found that, on thapsigargin treatment, SEC24A facilitates mitochondrial Ca^{2+} uptake from the ER, and that SEC24A facilitates the colocalization of mitochondria with tubules in the peripheral ER where Ca^{2+} signaling predominantly occurs in cells (Schwarz and Blower, 2016; Shibata et al., 2010). In the context of our findings, and since SEC24A functions at the ER, it is possible that SEC24A facilitates the formation of MAMs on the ER side of the physiological association between the two organelles in a manner analogous to how IRE1 modulates the MAM (Carreras-Sureda et al., 2019). This could potentially occur through a direct interaction with a protein such as IP3R (Rizzuto and Pozzan, 2006) on the ER, or indirectly through binding to another protein such as the ER resident protein, ERp44, which normally desensitizes IP3R activity when ER Ca^{2+} is depleted (Higo et al., 2005; Kiviluoto et al., 2013). Alternatively, SEC24A could facilitate the trafficking of a MAM inhibitor away from the ER in its canonical role as a cargo receptor. Further experimentation will be necessary to decipher the role of SEC24A in MAM formation and function.

Specificity of SEC24A-dependent cell death pathway

Our experiments with different *SEC24* knockout cells showed that SEC24A is the only SEC24 paralog necessary for cell death induced by SERCA inhibition. All four SEC24 paralogs are involved in COPII transport of secretory proteins from the ER to the Golgi in mammalian cells (Barlowe et al., 1994). Based on sequence homology, *SEC24A* and *SEC24B* belong to one group, while *SEC24C* and *SEC24D* comprise another (Pagano et al., 1999; Tang et al., 1999), and some redundancy between SEC24A and SEC24B has been observed for cargo transport (Wendeler et al., 2007). If the role of SEC24A in mediating cell death is dependent on its COPII transport function, our observation that SEC24B is not necessary for

Journal of Cell Science (2021) 134, jcs249276. doi:10.1242/jcs.249276

SERCA inhibition-induced cell death suggests that the cargo involved in SERCA inhibition-induced cell death binds SEC24A specifically. This is plausible since SEC24A is the only paralog that is necessary for transport of specific cargo with di-leucine motifs (Wendeler et al., 2007). Alternatively, it is also possible that SEC24A mediates thapsigargin-mediated cell death by a mechanism independent of its canonical role in COPII transport. Further experimentation will be required to explore this idea.

Our data also show that knocking out *SEC24A* partially protects against cell death induced by three different SERCA inhibitors, namely, thapsigargin, CPA and DTBHQ, but not by the topoisomerase inhibitor CPT. These findings, combined with our previous results showing that *SEC24A* KO cells are not protected against cell death induced by tunicamycin or brefeldin A (Chidawanyika et al., 2018), show that SEC24A is required for a process specifically initiated by SERCA inhibition. It is worth noting that *SEC24A* KO cells showed less survival when treated with CPA or DTBHQ than when treated with thapsigargin. It is known that thapsigargin binds to a different site on SERCA than CPA and DTBHQ (Xu et al., 2004). Thus, the observed variation in survival rates could be due to differences in how these inhibitors interact with SERCA or off-target effects. Regardless of these differences, our results identify SERCA inhibition as the event that specifically activates the SEC24A-dependent cell death pathway in HAP1 cells, most likely through mitochondrial Ca^{2+} overload, which subsequently causes apoptosis.

A hypothetical model of SEC24A-mediated cell death

Based on our results, we propose a hypothetical model for how SEC24A might mediate SERCA inhibition-induced cell death (Fig. 7). We used CPT to induce apoptosis without perturbing Ca^{2+} homeostasis and found that SEC24A only regulates apoptosis when triggered by SERCA inhibition, which is consistent with our previous finding that SEC24A acts upstream of the UPR (Chidawanyika et al., 2018). We therefore propose that SEC24A directly or indirectly facilitates MAM formation or function at the ER–mitochondria interface. Upon SERCA inhibition, Ca^{2+} flow from the ER into the mitochondria is facilitated by SEC24A, as shown by our direct measurements of Ca^{2+} levels in these organelles in WT cells. The close apposition of ER tubules, which are involved in Ca^{2+} signaling, and mitochondria is facilitated by SEC24A to allow for this Ca^{2+} flux. ER Ca^{2+} depletion activates the UPR, while mitochondrial Ca^{2+} overload results in a decrease in autophagic flux and activation of apoptosis.

Conclusion

In summary, we characterized the role of *SEC24A* in thapsigargin-induced cell death. Our work reveals a novel and surprising role for SEC24A in maintaining associations between and regulating the flow of Ca^{2+} between the ER and mitochondria, with important effects on apoptosis, autophagy and cell survival.

MATERIALS AND METHODS

Cell lines, plasmids and pharmaceutical agents

HAP1 cells were purchased from Horizon Discovery (Cambridge, UK) and the plasmids lentiCRISPRv2 (# 52961), pMD2.G (# 12259), psPAX (# 12260), and ER-GCamp6-150 (K_d=150 µM for Ca^{2+}) (# 86918), were obtained from Addgene (Cambridge, MA, USA). Cyto-R-GECO1 (K_d=0.48 µM for Ca^{2+}), and Mito-R-GECO1 (K_d=0.48 µM for Ca^{2+}) were gifts from Yuriy M. Usachev (University of Iowa Carver College of Medicine, Iowa City, IA, USA) and were previously described by Wu et al. (2014). ER-tagRFP and mito-BFP were gifts from Erik Snapp (Albert Einstein College of Medicine, New York, NY, USA) and Gia Voeltz (University of Colorado, Boulder, CO, USA). eGFP-tagged PTPIP51 was a gift from Christopher Miller (King's College, London, England, UK) and

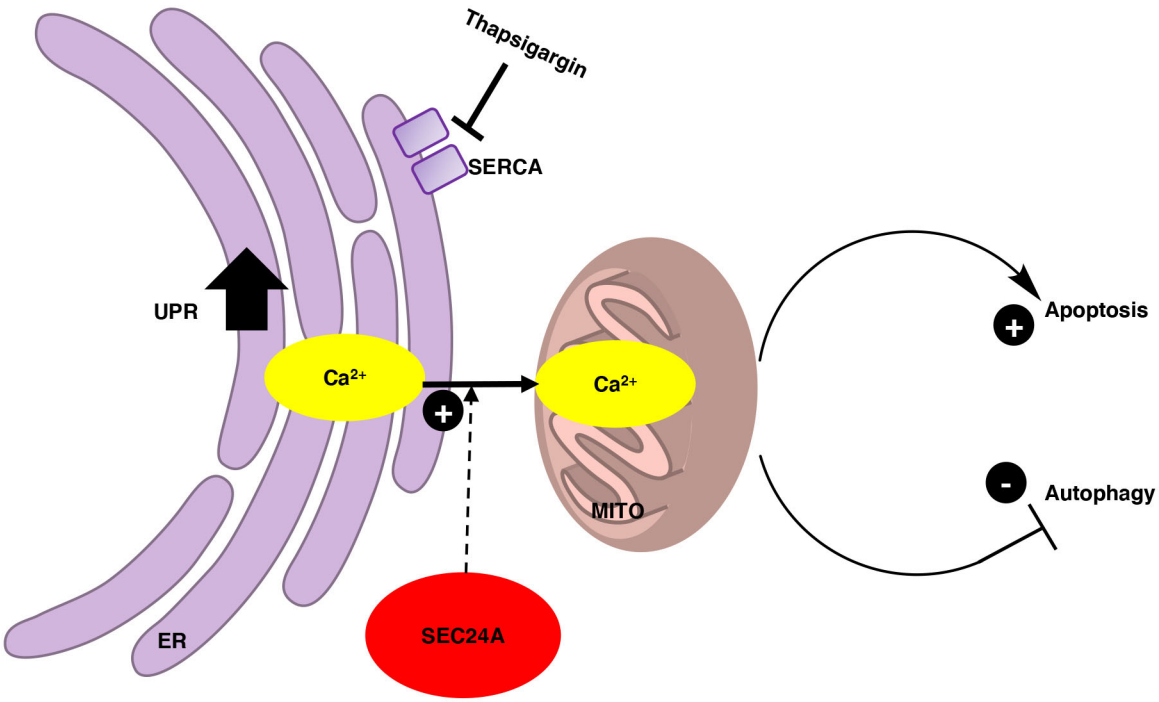

Fig. 7. Potential model for the role of SEC24A in SERCA inhibition-induced apoptosis. SEC24A facilitates associations between the ER and mitochondria and, therefore, SEC24A mediates ER-to-mitochondria Ca^{2+} flux upon SERCA inhibition. Mitochondrial Ca^{2+} overload results in autophagy inhibition and apoptosis induction in HAP1 cells. ER, endoplasmic reticulum; MITO, mitochondrion; SERCA, sarcoplasmic/endoplasmic reticulum Ca^{2+} ATPase pump. Image generated using ChemDraw software (PerkinElmer).

was previously described by Gomez-Suaga et al. (2017). Thapsigargin (TG) (catalog # T9033), cyclopiazonic acid (CPA) (catalog # C1530), and 2,5-di-tert-butylhydroquinone (DTBHQ) (catalog # 112976) for cytotoxicity assays were purchased from MilliporeSigma (Burlington, MA, USA). Thapsigargin (TG) (T7458) for Ca^{2+} measurements in confocal microscopy were obtained from Thermo Fisher Scientific (Waltham, MA, USA). Bafilomycin A1 (BafA1) (catalog # SML1661) and torin-1 (TRN1) (catalog # 10997) for autophagy-based assays were purchased from MilliporeSigma and Cayman Chemical (Ann Arbor, Michigan, USA), respectively. Camptothecin (CPT) (catalog # K121-5) and the pan-caspase inhibitor, Q-VD-OPh (catalog # A1901) for apoptosis-based assays were purchased from BioVision (Loma Linda, CA, USA) and Apexbio (Boston, MA, USA), respectively. All pharmaceutical agents were dissolved in DMSO (American Type Culture Collection, Manassas, VA, USA) unless otherwise specified. Final volumes of DMSO were kept at less than 1% (v/v) to prevent cytotoxicity from DMSO.

Cell culture and maintenance

HAP1 WT and *SEC24* paralog mutant cells were cultured in IMDM (MilliporeSigma) supplemented with 10% fetal bovine serum (FBS) (HyClone, UT, USA), 4 mM L-glutamine and 1× penicillin/streptomycin (Corning, Corning, NY, USA). This medium is complete IMDM. Cell lines were maintained at 37°C and 5% CO_2. Cell lines were monitored for mycoplasma contamination using the LookOut® Mycoplasma PCR detection kit (catalog # MP0035-1KT).

Generation of *SEC24* paralog mutant cell lines in HAP1 cells

Single-guide (sg)RNA sequences for targeted genes are shown in Table S1. sgRNAs were cloned into the lentiCRISPRv2 backbone as previously described (Joung et al., 2017) to generate specific lentiCRISPR plasmids. Using the U6 forward primer, the plasmids were Sanger sequenced to ensure that the sgRNAs were inserted in the lentiCRISPR plasmids correctly. To generate stable mutant cell lines, HAP1 cells were transfected with the lentiCRISPR, pMD2.G and psPAX plasmids using Turbofectin 8.0 (Origene, Rockville, MD, USA) per the manufacturer's protocol. Complete IMDM containing 1.5 µg/ml puromycin (MilliporeSigma) was used for a total of 5 days to select for transfected cells with refreshment of puromycin every 48 h. Monoclonal cell lines were isolated using serial dilution in 96-well plates (Corning).

Immunoblotting

Whole-cell lysates from cells of interest were isolated using PhosphoSafe Extraction Reagent (MilliporeSigma) supplemented with cOmplete, EDTA free protease inhibitor tablets (Roche, Mannheim, Germany) per the manufacturer's protocol. Lysates were run on 12% SDS polyacrylamide gels or Novex™ 4-20% Tris-Glycine gels (Thermo Fisher Scientific) and the separated proteins were transferred onto Immobilon-P PVDF membranes (IPVH00010) (MilliporeSigma) and blocked in 5% w/v milk in Tris-buffered saline with 0.1% Tween®20 (20 mM Tris-HCl, pH 7.6, 136 mM NaCl and 0.1% Tween®20) (TBST) buffer at room temperature for 1 h. After three 10 min washes in TBST, membranes were incubated in primary antibodies at 4°C overnight (see sections below). All secondary antibody incubations the following day were at room temperature for 1 h. After three 10 min washes in TBST, western blots were processed using SuperSignal West Femto Maximum Sensitivity Substrate (Thermo Fisher Scientific). This protocol for immunoblotting was carried out for all western blot processing and developing.

Immunoblotting and genotyping for mutation validation

Whole-cell lysates were isolated from ∼6×10^5 HAP1 WT and *SEC24* paralog mutant cells and run on 12% SDS polyacrylamide gels. The following antibodies were used: anti-SEC24A rabbit polyclonal antibody [1:1000 dilution in TBST with 5% (w/v) BSA; catalog # 9678S lot 1], anti-SEC24B (D7D6S) rabbit monoclonal antibody [1:1000 dilution in TBST with 5% (w/v) BSA; catalog # 12042S lot 1], anti-SEC24C (D9M4N) rabbit monoclonal antibody [1:1000 dilution with 5% (w/v) milk in TBST; catalog # 14676 lot 1], anti-SEC24D (D9M7L) rabbit monoclonal antibody [1:1000 dilution in 5% (w/v) milk in TBST; catalog # 14687 lot 1], and anti-rabbit IgG, HRP linked antibody [1:2000 dilution in 5% (w/v) milk in TBST; catalog # 7074] (Cell Signaling Technology, Danvers, MA, USA). Three *SEC24A* mutant cell lines that were generated as previously described (*SEC24A* mutants 1, 3 and 4) (Chidawanyika et al., 2018) were used in our experiments. *SEC24A* mutant 3, a confirmed knockout of *SEC24A* (Chidawanyika et al., 2018), was used for all comparisons to WT cells and is referred to as *SEC24A* KO throughout the manuscript. The other mutant cell lines that were used are *SEC24A* mutant 1 and *SEC24A* mutant 4 (Chidawanyika et al., 2018).

Immunoblotting for ER morphology

HAP1 WT and *SEC24A* KO cells (5×10^6 cells per plate) were seeded in 10 cm plates (Corning) 24 h before treatment with 0.095 µM TG or an equivalent volume of DMSO. After a 16 h treatment, whole-cell lysates were isolated and run on Novex™ 4-20% Tris-Glycine gels. The following antibodies were used for western blot processing: anti-Climp63 (G1/296) mouse monoclonal antibody [1:1000 dilution in 5% (w/v) milk in TBST; catalog # ENZ-ABS669-0100 lot 06031926] from Enzo Life Sciences (Farmingdale, NY, USA), anti-RTN4/NOGO antibody [1:1000 dilution in 5% (w/v) milk in TBST; catalog # 10950-1-AP] from Proteintech (Rosemont, IL, USA), anti-calnexin (C5C9) rabbit monoclonal antibody [1:1000 dilution in 5% (w/v) milk in TBST; catalog # 2679S lot 6], anti-rabbit IgG, horseradish peroxidase (HRP)-linked antibody [1:2000 dilution in 5% (w/v) milk in TBST; catalog # 7074], and anti-mouse IgG, HRP-linked antibody [1:2000 dilution in 5% (w/v) milk in TBST; catalog # 7076] (Cell Signaling Technology, Danvers, MA, USA).

Immunoblotting in apoptosis- and autophagy-based assays and for ER morphology detection

HAP1 WT and *SEC24* paralog mutant cells (5×10^6 cells per plate) were seeded in 10 cm plates (Corning) 24 h before stress induction. From stocks of 200 mM Q-VD-OPh and 160 µM BafA1 in DMSO, cells in each plate were treated with 5 ml of complete IMDM with 400 µM Q-VD-OPh, 100 nM BafA1, or DMSO (10 µl per plate which is equal in volume to the added Q-VD-OPh) for 1 h. From stocks of 100 µM TG, 2 mM CPT in DMSO, and 1 mM TRN1, 5 ml of complete IMDM containing 0.19 µM TG, 10 µM CPT, 2 µM TRN1 or DMSO (25 µl per plate which is equal in volume to the added CPT) was added such that final treatment concentrations per well were 200 µM Q-VD-OPh or 50 nM BafA1, with 0.095 µM TG, 5 µM CPT or 1 µM TRN1. Whole-cell lysates were isolated after a 24 h treatment for the apoptosis-based assay and after a 16 h treatment for the autophagy-based assay. Lysates were run on Novex™ 4–20% Tris-Glycine gels (Thermo Fisher Scientific) and visualized by western blotting using the following antibodies: anti-LC3A/B (D3U4C) XP® rabbit monoclonal antibody [1:1000 dilution in 5% (w/v) milk in TBST; catalog # 12741], anti-β-Tubulin [D2N5G; 1:5000 dilution in 5% (w/v) milk in TBST; catalog # 15115 lot 3], anti-PARP [1:1000 dilution in 5% (w/v) milk in TBST; catalog # 9542S lot 15], and anti-rabbit IgG, HRP-linked antibody [1:2000 dilution in 5% (w/v) milk in TBST; catalog # 7074; Cell Signaling Technology, Danvers, MA, USA].

Cytotoxicity assays against SERCA pump inhibitors and camptothecin

TG, CPA and DTBHQ were used to inhibit the SERCA pump in cells. Camptothecin was used to generate DNA damage in cells. Stock concentrations of 100 µM TG, 10 mM CPA, 50 mM DTBHQ and 2 mM CPT were prepared in DMSO. HAP1 WT cells were seeded in 12-well plates (Corning) 24 h before stress induction to allow for ∼60% confluence on the following day, and treated with a range of concentrations of TG, CPA, DTBHQ and CPT. After 3 days, cell viability was determined using Trypan Blue (Corning) and a hemocytometer to count live cells. Cytotoxicity curves were generated for each agent and at 0.095 µM TG, 80 µM CPA, 35 µM DTBHQ and 5 µM CPT ∼1% of the WT cells survived the stress. WT and *SEC24* paralog mutant cells were seeded in 12-well plates (1.5×10^5 cells per well) and treated with 0.095 µM TG, 80 µM CPA, 35 µM DTBHQ and 5 µM CPT after 24 h. After 3 days, cell viability was determined using Trypan Blue and a hemocytometer to count live cells. Data were plotted and analyzed using Prism software (GraphPad).

Journal of Cell Science (2021) 134, jcs249276. doi:10.1242/jcs.249276

Cell transfections for live and fixed cell confocal microscopy

The protocol used was adapted from Chakrabarti et al. (2018). HAP1 WT, *SEC24*A KO, *SEC24A* mutant 1, and *SEC24A* mutant 4 cells (8×10^5 cells per well) were seeded in six-well plates (Corning). After 24 h, Lipofectamine 2000 (Thermo Fisher Scientific) was used as per the manufacturer's protocol to transfect each cell line with ER-GCaMP6-150 (800 ng per well), cyto-R-GECO1 (500 ng per well), mito-R-GECO1 (500 ng per well), or ER-tagRFP (800 ng per well), mito-BFP (400 ng per well) and eGFP-tagged PTPIP51 (500 ng per well) for 6 h. Only WT cells were co-transfected with ER-tagRFP, mito-BFP and eGFP-tagged PTPIP51. Cells were washed once with Dulbecco's phosphate-buffered saline (PBS) (D8537; MilliporeSigma), trypsinized using trypsin (0.05%) in EDTA (0.02%) (59417C) (MilliporeSigma), and transferred to fibronectin (F1141; MilliporeSigma)-coated glass bottom MatTek dishes (P35G-1.5-14-C) (MatTek Corporation, Ashland, MA, USA) at $\sim8\times10^5$ cells per dish for the cells transfected with ER-GCamP6-150, cyto-R-GECO1 and mito-R-GECO1, and at $\sim2\times10^5$ cells per dish for cells that were co-transfected with ER-tagRFP and mito-BFP with or without eGFP-tagged PTPIP51. To prepare the dishes, the coverslips of the MatTek dishes were treated with 200 µl of 10 µg/ml fibronectin in PBS for 6 h at room temperature.

Cell preparation for live- and fixed-cell imaging by confocal microscopy

The protocol used was adapted from Chakrabarti et al. (2018). Cells that were transfected with ER-GCaMP6-150, cyto-R-GECO1 or mito-R-GECO1 were imaged as live cells. After 24 h of incubation on the MatTek dishes, the cells were imaged in 1 ml of DMEM without Phenol Red (Thermo Fisher Scientific), supplemented with 10% newborn calf serum (NCS) (HyClone). ER-GCamP6-150 (ER Ca^{2+}) fluorescence was collected at an excitation of 488 nm, while cyto-R-GECO1 (cytoplasm Ca^{2+}) and mito-R-GECO (mitochondria Ca^{2+}) fluorescence were collected at an excitation of 561 nm. At the end of the fourth frame of imaging, 1 ml of medium containing 4 µM TG (final concentration of 2 µM), 200 µM CPA (final concentration of 100 µM) or 200 µM DTBHQ (final concentration of 100 µM), was added to the dishes with continuous imaging.

Cells that were co-transfected with ER-tagRFP and mito-BFP, with or without eGFP-tagged PTPIP51 were imaged as fixed cells. After 24 h of incubation on the MatTek dishes, the cells were washed once with PBS. From an 8% glutaraldehyde (Electron Microscopy Sciences, Hatfield, PA, USA) stock, 1% glutaraldehyde was freshly prepared in BRB80 buffer (80 mM K-PIPES, 1 mM $MgCl_2$, and 1 mM K-EGTA). To fix the cells, 1 ml of the 1% glutaraldehyde buffer was added to each dish and the cells were incubated at room temperature for 10 min and then washed three times in PBS. A 2 mg/ml stock solution of sodium borohydride (MilliporeSigma) was freshly prepared in PBS and 1 ml of the sodium borohydride solution was added to each plate and after a 15 min incubation period at room temperature, the solution was removed from the cells. The process with the sodium borohydride solution was repeated two more times and then cells were washed in 1 ml of PBS three times. Cells were imaged in 1 ml PBS with the 561 nm laser and 595/25 emission filter for ER-tagRFP fluorescence, the 405 nm laser and 450/30 emission filter for mito-BFP fluorescence, and the 488 nm laser and 525/30 emission filter for eGFP-tagged PTPIP51 fluorescence.

Live- and fixed-cell imaging by confocal microscopy

A Dragonfly 302 spinning disk confocal (Andor Technology, Inc.) on a Nikon Ti-E base with an iXon Ultra 888 EMCCD camera and a Zyla 4.2 Mpixel sCMOS camera, and a Tokai Hit stage-top incubator at 37°C was used. A solid-state 405 smart diode 100-mW laser, a solid-state 488 OPSL smart laser 50-mW laser, and a solid-state 561 OPSL smart laser 50-mW laser were used (objective: 100×1.4 NA CFI Plan Apo; Nikon). Images were acquired using Fusion software (Andor Technology, Inc.).

Measurements of Ca^{2+} changes in live cells using ImageJ

Mean fluorescence values for ER-GCamP6-150, cyto-R-GECO, and mito-R-GECO over time were generated for individual cells using ImageJ (National Institutes of Health). Regions of interest (ROIs) were drawn around the fluorescent organelle(s) of interest based on the fluorescent probe that was used, and using the 'Time Series Analyzer V3' plugin, fluorescence values were collected. Since the background fluorescence of the iXon Ultra 888 EMCCD camera that was used to obtain the fluorescence data is 450, this value was background subtracted from all fluorescence values. The baseline fluorescence (F_0) of each cell was calculated from the mean fluorescence values of the first four frames. Fluorescence values for each time point after drug treatment (F) were normalized to F_0 to obtain the ratio F/F_0. Relative fluorescence (average F/F_0) values were then plotted against time.

Quantification of ER-mitochondria colocalization in tubular ER of WT, *SEC24A* KO, and PTPIP51 OX cells

WT and *SEC24A* KO cells that had been transfected with ER-tagRFP and mito-BFP and fixed in glutaraldehyde before imaging were analyzed using Image J. Overexpression of PTPIP51 is known to increase ER–mitochondria colocalization (Gomez-Suaga et al., 2017). HAP1 cells overexpressing PTPIP51 (PTPIP51 OX) were also transfected with ER-tagRFP and mito-BFP and they were used as a positive control. After subtracting background (rolling ball radius of 20.0 pixels), images of cells were normalized to the same brightness and contrast parameters to allow for adequate visualization of all of the cells before conversion to 8-bit images. Different brightness and contrast parameters were necessary for visualization of WT and *SEC24A* KO cells. A single *z*-stack that allowed for the cell under analysis to be at its flattest and most spread out was selected and this was often when the nucleus and nuclear membrane were clearly defined. The nuclear ER immediately surrounds the nucleus, while the peripheral ER occupies the rest of the cell (English et al., 2009). Rectangular ROIs were drawn around peripheral ER tubules in cells, which were identified by their 'reticular' appearance in the periphery or non-nuclear region of the cell. Colocalization of mitochondria with tubular ER was determined using the 'Colocalization' plugin. Images were converted into binary formats and the 'Analyze Particles' function was used to determine the total pixels of ER tubules, mitochondria, and colocalized ER and mitochondria in the selected ROIs. The pixels from the different ROIs were summed up. The total analyzed pixels were calculated by adding the total non-colocalized ER tubule pixels, the total non-colocalized mitochondria pixels and the total colocalized pixels. The proportions of colocalization relative to the total analyzed pixels were calculated for WT, *SEC24A* KO, PTPIP51 OX, *SEC24A* mutant 1 and *SEC24A* mutant 4 cells. For WT cells, 38 rectangular ROIs within 12 different cells containing a total number of 85,437 fluorescent pixels (ER and mitochondria) were analyzed. For *SEC24A* KO cells, 16 rectangular ROIs within 12 different cells containing a total number of fluorescent 54,167 pixels were analyzed. For PTPIP51 OX cells, 31 rectangular ROIs within 10 different cells containing a total number of 25,959 fluorescent pixels were analyzed. For *SEC24A* mutant 1 cells, 33 rectangular ROIs within 26 different cells containing a total number of 14,364 fluorescent pixels were analyzed. For *SEC24A* mutant 4 cells, 41 rectangular ROIs within 27 different cells containing a total number of 20,376 fluorescent pixels were analyzed. Two-sided, two-sample tests of proportions were run using Stata 15.1 to assess whether the proportion of colocalized pixels relative to total analyzed pixels in WT cells was different to the proportions in *SEC24A* KO, PTPIP51 OX, *SEC24A* mutant 1 and *SEC24A* mutant 4 cells.

Morphological analyses of mitochondrial length and number in WT and *SEC24A* KO cells

WT and *SEC24A* KO cells that were transfected with mito-BFP and fixed in glutaraldehyde before imaging were analyzed in ImageJ for mitochondrial length and number using a morphometric protocol adapted from Lee et al. (2016). Maximum intensity projections were acquired from *z*-stacks and a 42.25 μm^2 box was selected in the peripheral ER tubular region of the cell as the ROI. After image conversion to 8-bit and background subtraction (rolling ball radius of 20.0 pixels), images were converted into binary form. The number of mitochondria were counted making sure to count any connected mitochondria as a single mitochondrion. The 'Analyze Particles' function was used to determine the total number of pixels and the total area of the ROI. For WT cells, 23 ROIs in 23 cells were analyzed. For *SEC24A* KO cells, 35 ROIs in 35 cells were analyzed. Mean mitochondrial length

was represented graphically as mean area per mitochondrion for both WT and *SEC24A* KO cells (Lee et al., 2016). The number of mitochondria in WT and *SEC24A* KO cells were quantified and represented graphically as the number of mitochondria per ROI (Lee et al., 2016).

Cytotoxicity assays with apoptosis inhibition and induction

HAP1 WT cells (1.5×10^5 cells per well) were seeded in 12-well plates and incubated for 24 h at 37°C, 5% CO_2. For apoptosis inhibition assays, from a stock of 200 mM Q-VD-OPh in DMSO, cells in each well were treated with 500 µl of complete IMDM with 400 µM Q-VD-OPh or DMSO (1 µl per well which is equal in volume to the added Q-VD-OPh) for 1 h. From stocks of 100 µM TG and 2 mM CPT in DMSO, 500 µl of complete IMDM containing 0.19 µM TG, 10 µM CPT or DMSO (2.5 µl per well which is equal in volume to the added CPT) was added such that final treatment concentrations per well were 200 µM Q-VD-OPh with 0.095 µM TG or 5 µM CPT. Cell survival was calculated as the percentage of the surviving cells in Q-VD-OPh- or DMSO-treated cells. For apoptosis induction assays, from a stock of 2 mM CPT in DMSO, 1 ml of complete IMDM containing 5 µM CPT or DMSO (5 µl per well which is equal in volume to the added CPT) was added. After 3 days of treatment, cell viability was determined using Trypan Blue and a hemocytometer. Cell survival was calculated as a percentage of the surviving cells in DMSO-treated cells. Data were plotted and analyzed using Prism software.

Quantification of western blots using ImageJ

Protein bands on western blots were analyzed and quantified using ImageJ. An ROI was generated using the largest band, and this ROI was used to measure all band intensities. A background intensity value was obtained using the ROI in a randomly selected area of the blot that did not have any distinct bands. Background intensity was calculated and subtracted from each band value. For quantification of PARP protein bands on western blots, four replicates were obtained from two biological replicates, and two technical replicates from developing the blots at different exposures. For quantification of PARP cleavage, cleaved PARP in treatments was normalized to cleaved PARP in DMSO-treated control in the same cell type using subtraction. Data were plotted using the GraphPad Prism software.

Statistical analysis

Data are presented as mean±s.e.m. Analysis of statistical significance was determined using one-way ANOVA or Student's *t*-test (GraphPad Prism software) as appropriate for each figure unless otherwise specified. Statistical significance was determined at the 0.05 level and a normal distribution of the data was assumed.

Acknowledgements

We thank Dartmouth College Molecular Biology Core Facility and Tufts University Core Facility core facilities for sequencing services. We also thank Judith Rees for her assistance with statistical analyses.

Competing interests

The authors declare no competing or financial interests.

Author contributions

Conceptualization: T.C., R.C., S.S.; Methodology: T.C., R.C., S.S.; Validation: T.C., R.C., K.S.B.; Formal analysis: T.C., R.C.; Investigation: T.C., R.C., K.S.B., S.S.; Resources: H.N.H., S.S.; Writing - original draft: T.C., S.S.; Writing - review & editing: T.C., S.S.; Visualization: T.C., R.C.; Supervision: H.N.H., S.S.; Project administration: S.S.; Funding acquisition: S.S.

Funding

This work was funded by the National Institutes of Health (R01NS102301, R01NS117276 and R01NS118796 to S.S., IDeA award to Dartmouth BioMT P20-GM113132, 5T32A1007519-22 to K.S.B.). Deposited in PMC for release after 12 months.

Supplementary information

Supplementary information available online at https://jcs.biologists.org/lookup/doi/10.1242/jcs.249276.supplemental

References

Bagur, R. and Hajnóczky, G. (2017). Intracellular Ca^{2+} Sensing: its role in calcium homeostasis and signaling. *Mol. Cell* **66**, 780-788. doi:10.1016/j.molcel.2017.05.028

Barlowe, C., Orci, L., Yeung, T., Hosobuchi, M., Hamamoto, S., Salama, N., Rexach, M. F., Ravazzola, M., Amherdt, M. and Schekman, R. (1994). COPII: a membrane coat formed by Sec proteins that drive vesicle budding from the endoplasmic reticulum. *Cell* **77**, 895-907. doi:10.1016/0092-8674(94)90138-4

Berridge, M. J., Lipp, P. and Bootman, M. D. (2000). The versatility and universality of calcium signalling. *Nat. Rev. Mol. Cell Biol.* **1**, 11-21. doi:10.1038/35036035

Burgoyne, T., Patel, S. and Eden, E. R. (2015). Calcium signaling at ER membrane contact sites. *Biochim. Biophys. Acta* **1853**, 2012-2017. doi:10.1016/j.bbamcr.2015.01.022

Cárdenas, C. and Foskett, J. K. (2012). Mitochondrial Ca^{2+} signals in autophagy. *Cell Calcium* **52**, 44-51. doi:10.1016/j.ceca.2012.03.001

Carette, J. E., Raaben, M., Wong, A. C., Herbert, A. S., Obernosterer, G., Mulherkar, N., Kuehne, A. I., Kranzusch, P. J., Griffin, A. M., Ruthel, G. et al. (2011). Ebola virus entry requires the cholesterol transporter Niemann-Pick C1. *Nature* **477**, 340-343. doi:10.1038/nature10348

Carreras-Sureda, A., Jaña, F., Urra, H., Durand, S., Mortenson, D. E., Sagredo, A., Bustos, G., Hazari, Y., Ramos-Fernández, E., Sassano, M. L. et al. (2019). Publisher correction: non-canonical function of IRE1α determines mitochondria-associated endoplasmic reticulum composition to control calcium transfer and bioenergetics. *Nat. Cell Biol.* **21**, 913. doi:10.1038/s41556-019-0355-9

Chakrabarti, R., Ji, W.-K., Stan, R. V., de Juan Sanz, J., Ryan, T. A. and Higgs, H. N. (2018). INF2-mediated actin polymerization at the ER stimulates mitochondrial calcium uptake, inner membrane constriction, and division. *J. Cell Biol.* **217**, 251-268. doi:10.1083/jcb.201709111

Chen, A. Y. and Liu, L. F. (1994). DNA topoisomerases: essential enzymes and lethal targets. *Annu. Rev. Pharmacol. Toxicol.* **34**, 191-218. doi:10.1146/annurev.pa.34.040194.001203

Chidawanyika, T., Sergison, E., Cole, M., Mark, K. and Supattapone, S. (2018). SEC24A identified as an essential mediator of thapsigargin-induced cell death in a genome-wide CRISPR/Cas9 screen. *Cell Death Discov.* **4**, 115. doi:10.1038/s41420-018-0135-5

Coe, H. and Michalak, M. (2009). Calcium binding chaperones of the endoplasmic reticulum. *Gen. Physiol. Biophys.* **28** Spec No Focus, F96-F103.

English, A. R., Zurek, N. and Voeltz, G. K. (2009). Peripheral ER structure and function. *Curr. Opin. Cell Biol.* **21**, 596-602. doi:10.1016/j.ceb.2009.04.004

Filippi-Chiela, E. C., Viegas, M. S., Thomé, M. P., Buffon, A., Wink, M. R. and Lenz, G. (2016). Modulation of autophagy by calcium signalosome in human disease. *Mol. Pharmacol.* **90**, 371-384. doi:10.1124/mol.116.105171

Goeger, D. E., Riley, R. T., Dorner, J. W. and Cole, R. J. (1988). Cyclopiazonic acid inhibition of the Ca2+-transport ATPase in rat skeletal muscle sarcoplasmic reticulum vesicles. *Biochem. Pharmacol.* **37**, 978-981. doi:10.1016/0006-2952(88)90195-5

Gomez-Suaga, P., Paillusson, S., Stoica, R., Noble, W., Hanger, D. P. and Miller, C. C. J. (2017). The ER-mitochondria tethering complex VAPB-PTPIP51 regulates autophagy. *Curr. Biol.* **27**, 371-385. doi:10.1016/j.cub.2016.12.038

Gordon, P. B., Holen, I., Fosse, M., Røtnes, J. S. and Seglen, P. O. (1993). Dependence of hepatocytic autophagy on intracellularly sequestered calcium. *J. Biol. Chem.* **268**, 26107-26112. doi:10.1016/S0021-9258(19)74287-2

Gürkan, C., Stagg, S. M., Lapointe, P. and Balch, W. E. (2006). The COPII cage: unifying principles of vesicle coat assembly. *Nat. Rev. Mol. Cell Biol.* **7**, 727-738. doi:10.1038/nrm2025

Higo, T., Hattori, M., Nakamura, T., Natsume, T., Michikawa, T. and Mikoshiba, K. (2005). Subtype-specific and ER lumenal environment-dependent regulation of inositol 1,4,5-trisphosphate receptor type 1 by ERp44. *Cell* **120**, 85-98. doi:10.1016/j.cell.2004.11.048

Joung, J., Konermann, S., Gootenberg, J. S., Abudayyeh, O. O., Platt, R. J., Brigham, M. D., Sanjana, N. E. and Zhang, F. (2017). Genome-scale CRISPR-Cas9 knockout and transcriptional activation screening. *Nat. Protoc.* **12**, 828-863. doi:10.1038/nprot.2017.016

Jozsef, L., Tashiro, K., Kuo, A., Park, E. J., Skoura, A., Albinsson, S., Rivera-Molina, F., Harrison, K. D., Iwakiri, Y., Toomre, D. et al. (2014). Reticulon 4 is necessary for endoplasmic reticulum tubulation, STIM1–Orai1 coupling, and store-operated calcium entry. *J. Biol. Chem.* **289**, 9380-9395. doi:10.1074/jbc.M114.548602

Kaufmann, S. H., Desnoyers, S., Ottaviano, Y., Davidson, N. E. and Poirier, G. G. (1993). Specific proteolytic cleavage of poly(ADP-ribose) polymerase: an early marker of chemotherapy-induced apoptosis. *Cancer Res.* **53**, 3976-3985.

Kita, H., Okamoto, K., Kushima, R., Kawauchi, A. and Chano, T. (2015). Dimethyl sulfoxide induces chemotherapeutic resistance in the treatment of testicular embryonal carcinomas. *Oncol. Lett.* **10**, 661-666. doi:10.3892/ol.2015.3306

Kiviluoto, S., Vervliet, T., Ivanova, H., Decuypere, J.-P., De Smedt, H., Missiaen, L., Bultynck, G. and Parys, J. B. (2013). Regulation of inositol 1,4,5–trisphosphate receptors during endoplasmic reticulum stress. *Biochim. Biophys. Acta* **1833**, 1612-1624. doi:10.1016/j.bbamcr.2013.01.026

Kowaltowski, A. J., Menezes-Filho, S. L., Assali, E. A., Gonçalves, I. G., Cabral-Costa, J. V., Abreu, P., Miller, N., Nolasco, P., Laurindo, F. R. M., Bruni-Cardoso, A. et al. (2019). Mitochondrial morphology regulates organellar Ca^{2+} uptake and changes cellular Ca^{2+} homeostasis. *FASEB J.* **33**, 13176-13188. doi:10.1096/fj.201901136R

Le Rhun, Y., Kirkland, J. B. and Shah, G. M. (1998). Cellular responses to DNA damage in the absence of Poly(ADP-ribose) polymerase. *Biochem. Biophys. Res. Commun.* **245**, 1-10. doi:10.1006/bbrc.1998.8257

Lee, J. E., Westrate, L. M., Wu, H., Page, C. and Voeltz, G. K. (2016). Multiple dynamin family members collaborate to drive mitochondrial division. *Nature* **540**, 139-143. doi:10.1038/nature20555

Lytton, J., Westlin, M. and Hanley, M. R. (1991). Thapsigargin inhibits the sarcoplasmic or endoplasmic reticulum Ca-ATPase family of calcium pumps. *J. Biol. Chem.* **266**, 17067-17071. doi:10.1016/S0021-9258(19)47340-7

Mahalingam, D., Wilding, G., Denmeade, S., Sarantopoulas, J., Cosgrove, D., Cetnar, J., Azad, N., Bruce, J., Kurman, M., Allgood, V. E. et al. (2016). Mipsagargin, a novel thapsigargin-based PSMA-activated prodrug: results of a first-in-man phase I clinical trial in patients with refractory, advanced or metastatic solid tumours. *Br. J. Cancer* **114**, 986-994. doi:10.1038/bjc.2016.72

McCormack, J. G., Halestrap, A. P. and Denton, R. M. (1990). Role of calcium ions in regulation of mammalian intramitochondrial metabolism. *Physiol. Rev.* **70**, 391-425. doi:10.1152/physrev.1990.70.2.391

Mizushima, N. and Yoshimori, T. (2007). How to interpret LC3 immunoblotting. *Autophagy* **3**, 542-545. doi:10.4161/auto.4600

Mizushima, N., Yoshimori, T. and Levine, B. (2010). Methods in mammalian autophagy research. *Cell* **140**, 313-326. doi:10.1016/j.cell.2010.01.028

Moore, G. A., McConkey, D. J., Kass, G. E. N., O'Brien, P. J. and Orrenius, S. (1987). 2,5-Di(tert-butyl)-1,4-benzohydroquinone — a novel inhibitor of liver microsomal Ca^{2+} sequestration. *FEBS Lett.* **224**, 331-336. doi:10.1016/0014-5793(87)80479-9

Orrenius, S., Zhivotovsky, B. and Nicotera, P. (2003). Regulation of cell death: the calcium-apoptosis link. *Nat. Rev. Mol. Cell Biol.* **4**, 552-565. doi:10.1038/nrm1150

Orrenius, S., Gogvadze, V. and Zhivotovsky, B. (2015). Calcium and mitochondria in the regulation of cell death. *Biochem. Biophys. Res. Commun.* **460**, 72-81. doi:10.1016/j.bbrc.2015.01.137

Oslowski, C. M. and Urano, F. (2011). Measuring ER stress and the unfolded protein response using mammalian tissue culture system. *Methods Enzymol.* **490**, 71-92. doi:10.1016/B978-0-12-385114-7.00004-0

Pagano, A., Letourneur, F., Garcia-Estefania, D., Carpentier, J.-L., Orci, L. and Paccaud, J.-P. (1999). Sec24 proteins and sorting at the endoplasmic reticulum. *J. Biol. Chem.* **274**, 7833-7840. doi:10.1074/jbc.274.12.7833

Pinton, P., Giorgi, C., Siviero, R., Zecchini, E. and Rizzuto, R. (2008). Calcium and apoptosis: ER-mitochondria Ca^{2+} transfer in the control of apoptosis. *Oncogene* **27**, 6407-6418. doi:10.1038/onc.2008.308

Qian, T., Herman, B. and Lemasters, J. J. (1999). The mitochondrial permeability transition mediates both necrotic and apoptotic death of hepatocytes exposed to Br-A23187. *Toxicol. Appl. Pharmacol.* **154**, 117-125. doi:10.1006/taap.1998.8580

Raffaello, A., Mammucari, C., Gherardi, G. and Rizzuto, R. (2016). Calcium at the center of cell signaling: interplay between endoplasmic reticulum, mitochondria, and lysosomes. *Trends Biochem. Sci.* **41**, 1035-1049. doi:10.1016/j.tibs.2016.09.001

Rizzuto, R. and Pozzan, T. (2006). Microdomains of intracellular Ca^{2+}: molecular determinants and functional consequences. *Physiol. Rev.* **86**, 369-408. doi:10.1152/physrev.00004.2005

Rizzuto, R., Bastianutto, C., Brini, M., Murgia, M. and Pozzan, T. (1994). Mitochondrial Ca^{2+} homeostasis in intact cells. *J. Cell Biol.* **126**, 1183-1194. doi:10.1083/jcb.126.5.1183

Rizzuto, R., Marchi, S., Bonora, M., Aguiari, P., Bononi, A., De Stefani, D., Giorgi, C., Leo, S., Rimessi, A., Siviero, R. et al. (2009). Ca^{2+} transfer from the ER to mitochondria: when, how and why. *Biochim. Biophys. Acta* **1787**, 1342-1351. doi:10.1016/j.bbabio.2009.03.015

Ron, D. and Walter, P. (2007). Signal integration in the endoplasmic reticulum unfolded protein response. *Nat. Rev. Mol. Cell Biol.* **8**, 519-529. doi:10.1038/nrm2199

Sanchez-Alcazar, J. A., Ault, J. G., Khodjakov, A. and Schneider, E. (2000). Increased mitochondrial cytochrome c levels and mitochondrial hyperpolarization precede camptothecin-induced apoptosis in Jurkat cells. *Cell Death Differ.* **7**, 1090-1100. doi:10.1038/sj.cdd.4400740

Schwarz, D. S. and Blower, M. D. (2016). The endoplasmic reticulum: structure, function and response to cellular signaling. *Cell Mol. Life Sci.* **73**, 79-94. doi:10.1007/s00018-015-2052-6

Shibata, Y., Shemesh, T., Prinz, W. A., Palazzo, A. F., Kozlov, M. M. and Rapoport, T. A. (2010). Mechanisms determining the morphology of the peripheral ER. *Cell* **143**, 774-788. doi:10.1016/j.cell.2010.11.007

Shigekawa, M., Wakabayashi, S. and Nakamura, H. (1983). Reaction mechanism of Ca2+-dependent adenosine triphosphatase of sarcoplasmic reticulum. ATP hydrolysis with CaATP as a substrate and role of divalent cation. *J. Biol. Chem.* **258**, 8698-8707. doi:10.1016/S0021-9258(18)32113-6

Spamer, C., Heilmann, C. and Gerok, W. (1987). Ca2+-activated ATPase in microsomes from human liver. *J. Biol. Chem.* **262**, 7782-7789. doi:10.1016/S0021-9258(18)47636-3

Supattapone, S., Worley, P. F., Baraban, J. M. and Snyder, S. H. (1988). Solubilization, purification, and characterization of an inositol trisphosphate receptor. *J. Biol. Chem.* **263**, 1530-1534. doi:10.1016/S0021-9258(19)57336-7

Tabas, I. and Ron, D. (2011). Integrating the mechanisms of apoptosis induced by endoplasmic reticulum stress. *Nat. Cell Biol.* **13**, 184-190. doi:10.1038/ncb0311-184

Tang, B. L., Kausalya, J., Low, D. Y. H., Lock, M. L. and Hong, W. (1999). A family of mammalian proteins homologous to yeast Sec24p. *Biochem. Biophys. Res. Commun.* **258**, 679-684. doi:10.1006/bbrc.1999.0574

Traganos, F., Seiter, K., Feldman, E., Halicka, H. D. and Darzynkiewicz, Z. (1996). Induction of apoptosis by camptothecin and topotecan. *Ann. N. Y. Acad. Sci.* **803**, 101-110. doi:10.1111/j.1749-6632.1996.tb26380.x

Verheijen, M., Lienhard, M., Schrooders, Y., Clayton, O., Nudischer, R., Boerno, S., Timmermann, B., Selevsek, N., Schlapbach, R., Gmuender, H. et al. (2019). DMSO induces drastic changes in human cellular processes and epigenetic landscape in vitro. *Sci. Rep.* **9**, 4641. doi:10.1038/s41598-019-40660-0

Wendeler, M. W., Paccaud, J.-P. and Hauri, H.-P. (2007). Role of Sec24 isoforms in selective export of membrane proteins from the endoplasmic reticulum. *EMBO Rep.* **8**, 258-264. doi:10.1038/sj.embor.7400893

Wu, J., Prole, D. L., Shen, Y., Lin, Z., Gnanasekaran, A., Liu, Y., Chen, L., Zhou, H., Chen, S. R., Usachev, Y. M. et al. (2014). Red fluorescent genetically encoded Ca2+ indicators for use in mitochondria and endoplasmic reticulum. *Biochem. J.* **464**, 13-22. doi:10.1042/BJ20140931

Xu, C., Ma, H., Inesi, G., Al-Shawi, M. K. and Toyoshima, C. (2004). Specific structural requirements for the inhibitory effect of thapsigargin on the Ca2+ ATPase SERCA. *J. Biol. Chem.* **279**, 17973-17979. doi:10.1074/jbc.M313263200

Xu, C., Bailly-Maitre, B. and Reed, J. C. (2005). Endoplasmic reticulum stress: cell life and death decisions. *J. Clin. Invest.* **115**, 2656-2664. doi:10.1172/JCI26373